

PAPER

## Establishing the quantum supremacy frontier with a 281 Pflop/s simulation

To cite this article: Benjamin Villalonga *et al* 2020 *Quantum Sci. Technol.* **5** 034003

View the [article online](#) for updates and enhancements.

### You may also like

- [Methods for classically simulating noisy networked quantum architectures](#)  
Iskren Vankov, Daniel Mills, Petros Wallden *et al.*
- [Quantum information processing with superconducting circuits: a review](#)  
G Wendin
- [Verifying commuting quantum computations via fidelity estimation of weighted graph states](#)  
Masahito Hayashi and Yuki Takeuchi



**IOP | ebooks™**

Bringing together innovative digital publishing with leading authors from the global scientific community.

Start exploring the collection—download the first chapter of every title for free.

# Quantum Science and Technology



## PAPER

# Establishing the quantum supremacy frontier with a 281 Pflop/s simulation

Benjamin Villalonga<sup>1,2,3</sup>, Dmitry Lyakh<sup>4,5</sup>, Sergio Boixo<sup>6</sup>, Hartmut Neven<sup>6</sup>, Travis S Humble<sup>4</sup>, Rupak Biswas<sup>1</sup>, Eleanor G Rieffel<sup>1</sup>, Alan Ho<sup>6</sup> and Salvatore Mandrà<sup>1,7,8</sup> 

<sup>1</sup> Quantum Artificial Intelligence Lab. (QuAIL), NASA Ames Research Center, Moffett Field, CA 94035, United States of America

<sup>2</sup> USRA Research Institute for Advanced Computer Science (RIACS), 615 National, Mountain View, California 94043, United States of America

<sup>3</sup> Institute for Condensed Matter Theory and Department of Physics, University of Illinois at Urbana-Champaign, Urbana, IL 61801, United States of America

<sup>4</sup> Quantum Computing Institute, Oak Ridge National Laboratory, Oak Ridge, TN, 37831, United States of America

<sup>5</sup> Scientific Computing, Oak Ridge Leadership Computing, Oak Ridge National Laboratory, Oak Ridge, TN, 37831, United States of America

<sup>6</sup> Google Inc., Venice, CA 90291, United States of America

<sup>7</sup> Stinger Ghaffarian Technologies Inc., 7701 Greenbelt Rd., Suite 400, Greenbelt, MD 20770, United States of America

<sup>8</sup> Author to whom any correspondence should be addressed.

E-mail: [salvatore.mandra@nasa.gov](mailto:salvatore.mandra@nasa.gov)

**Keywords:** quantum simulation, quantum circuits, HPC

## Abstract

Noisy intermediate-scale quantum (NISQ) computers are entering an era in which they can perform computational tasks beyond the capabilities of the most powerful classical computers, thereby achieving ‘quantum supremacy’, a major milestone in quantum computing. NISQ supremacy requires comparison with a state-of-the-art classical simulator. We report HPC simulations of hard random quantum circuits (RQC), which have been recently used as a benchmark for the first experimental demonstration of quantum supremacy, sustaining an average performance of 281 Pflop/s (true single precision) on Summit, currently the fastest supercomputer in the world. These simulations were carried out using qFlex, a tensor-network-based classical high-performance simulator of RQCs. Our results show an advantage of many orders of magnitude in energy consumption of NISQ devices over classical supercomputers. In addition, we propose a standard benchmark for NISQ computers based on qFlex.

## 1. Introduction and motivations

As we approach the end of Moore’s law, there is growing urgency to develop alternative computational models. Examples are beyond von Neumann architectures and beyond CMOS hardware. Since Feynman envisioned the possibility of using quantum physics for computation [1, 2], many theoretical and technological advances have been made. Quantum computing is both beyond von Neumann and beyond CMOS. It represents the most potentially transformative technology in computing.

Recent experiments have underscored the remarkable potential for quantum computing to offer new capabilities for computation. Experiments using superconducting electronic circuits have shown that control over quantum mechanics can be scaled to modest sizes with relatively good accuracy [3–7]. By exercising control over quantum physical systems, quantum computers are expected to accelerate the time to solution and/or accuracy of a variety of different applications [1, 8–14], while simultaneously reducing power consumption. For instance, important encryption protocols such as RSA, which is widely used in private and secure communications, can theoretically be broken using quantum computers [15]. Moreover, quantum simulation problems, including new material design and drug discovery, could be accelerated using quantum processors [1, 11–14, 16].

However, building a universal, fault tolerant quantum computer is, at the moment, a long-term goal driven by strong theoretical [17–19] and experimental [3, 4, 20] evidence. Nonetheless, despite the lack of error correction mechanisms to run arbitrary quantum algorithms, noisy intermediate-scale quantum (NISQ) devices of about 50–100 qubits are expected to perform certain tasks which surpass the capabilities of classical high-performance computer systems [18–33], therefore achieving quantum supremacy. Examples of NISQ devices are the 53-qubit IBM Rochester QPU [34], and the 53-qubit Google Sycamore QPU [7]. Both NISQ devices are ‘digital’ universal quantum computers, namely they perform a universal set of discrete operations (‘gates’) on qubits. Quantum algorithms are translated into quantum circuits and run on the NISQ device. The ‘depth’ of quantum circuits is defined as the number of clock cycles, where each clock cycle is composed of gate operations executed on distinct qubits. Given the noisy nature of NISQ devices, only shallow or low depth quantum circuits can be run.

An extensive body of work in complexity theory in the context of ‘quantum supremacy’ and random circuit sampling (RCS) supports the conclusion that ideal quantum computers can break the strong Church–Turing thesis by performing computations that cannot be reduced in polynomial time to any classical computational model [18, 19, 26, 35–39]. The milestone of experimentally demonstrating quantum supremacy was recently achieved by Google with its Sycamore processor [7].

Here we present a state-of-the-art classical high-performance simulator of large random quantum circuits (RQCs), called qFlex, and propose a systematic benchmark for noisy intermediate-scale quantum (NISQ) devices [22]. qFlex makes use of efficient single-precision matrix–matrix multiplications and an optimized tensor transpose kernel on NVIDIA GPUs. It utilizes efficient asynchronous pipelined task-based execution of tensor contractions implemented in its portable computational backend (TAL-SH library) that can run on both multicore CPU and NVIDIA GPU architectures. Our GPU implementation of qFlex reaches a peak performance efficiency of 92% and delivers a sustained absolute performance efficiency of 68% in simulations spanning the entire Summit supercomputer (281 Pflop/s single precision without mixed-precision acceleration). Due to our communication-avoiding algorithm, this performance is stable with respect to the number of utilized nodes, thus also demonstrating excellent strong scaling.

### 1.1. RCS protocol

While these demonstrations show progress in the development of quantum computing, it remains challenging to compare alternative quantum computing platforms and to evaluate advances with respect to the current dominant (classical) computing paradigm. The leading proposal to fulfill this critical need is quantum random circuit sampling (RCS) [7, 18, 26, 37, 39], that is, to approximately sample bitstrings from the output distribution generated by a random quantum circuit. This is a ‘hello world’ program for quantum computers, because it is the task they are designed to do. This proposal also counts with the strongest theoretical support in complexity theory for an exponential separation between classical and quantum computation [19, 37]. It is precisely this ‘hello world’ program that was used in reference [7] to demonstrate quantum supremacy. Classically, it requires a simulation of the quantum computation, and the computational cost increases exponentially in the number of qubits for quantum circuits of sufficient depth. Storing the wave function from the output of a random quantum circuit with 40 qubits requires 8.8 TB at single precision ( $2^{40} \times 8$  bytes), and 50 qubits require 9 PB. Although new algorithms such as qFlex are designed to avoid these memory requirements, calculating the necessary large number of probabilities for the output bitstrings of quantum circuits of sufficient depth with 40 qubits or more can only be achieved with HPC resources.

The RCS protocol to benchmark NISQ computers consists of the following steps:

- (a) Generate random circuits fitted to a given NISQ architecture,
- (b) Execute random circuits, collecting bitstrings, time to solution, and energy consumption of the quantum computer,
- (c) Calculate probabilities of collected bitstrings using a classical simulation (qFlex) to measure the NISQ performance or fidelity (see below),
- (d) Perform a classical noisy simulation (qFlex) based on calculated (point 3) fidelity to collect equivalent classical computational metrics of relevance—total floating point operations/time-to-solution/power consumption.

The NISQ fidelity (item 3 above) of the RCS protocol can be estimated using qFlex to calculate the probabilities of the bitstrings obtained in the NISQ experiment. This is done by using the cross-entropy benchmarking (XEB), see figure 1 and reference [18]. Then, the so-called heavy output generation (HOG) score is also calculated with the same data [37]. Note that items 3 and 4 above cannot be performed once the quantum supremacy threshold has been surpassed. In that case, the fidelity of the quantum computer can only be estimated for easier instances of the RQCs, an estimate that proves accurate in practice [7]. An

```

circuit = RandomCircuit()
size = 10**6
# Run on real hardware.
samples = Sample(circuit, size)
# Determine probabilities with simulation
p = 1
for s in samples:
    # EXPENSIVE!
    p *= Probability(circuit, s)
# Derive cross entropy.
cross_entropy = -log(p) / size

```

**Figure 1.** Cross-entropy benchmarking (XEB) pseudo-code.

alternative benchmark for NISQ devices called ‘quantum volume’ [40] is also based on RCS with additional requirements in the model circuits (item 1 above).

## 1.2. Motivation for RCS as a standard benchmark

The purpose of benchmarking quantum computers is twofold: to objectively rank NISQ computers as well as to understand quantum computational power in terms of equivalent ‘classical computing’ capability. Therefore, to achieve the above objectives, a good benchmark for NISQ computers must have the following properties:

- *A good predictor of NISQ algorithm performance.* In the classical computing world, Linpack is used as a benchmark for HPC Top-500 and serves as a relatively good predictor of application performance. Similarly, RCS serves as a good ‘multi-qubit’ benchmark because:
  - \* The computation is well defined,
  - \* The computation requires careful control of multiple qubits,
  - \* It measures the fidelity of an NISQ computer using cross-entropy benchmarking (XEB) [7, 18, 20]
  - \* Works for any set of universal gates.
- *Estimating the equivalent classical worst-case computation resources* with commonly used metrics such as time-to-solution speedup, equivalent floating point operations, and equivalent power usage metrics. Typically, advancements in classical algorithms could invalidate a quantum benchmark result. A key feature of RCS is that there is a large body of theory in computational complexity against an efficient classical algorithm [18, 19, 26, 35–39]. Furthermore, qFlex for RCS requires computational resources proportional to the sampling fidelity, taking into account NISQ errors [31, 32]. Lastly, quantum random circuits produce quasi-maximal entanglement in the ideal case.
- *Architectural neutrality.* Different architectures (e.g. ion traps vs superconducting qubits) have very different performance capabilities in terms of:
  - \* Number of qubits
  - \* Types of gates and fidelity
  - \* Connectivity
  - \* Number of qubits per multi-qubit operation
  - \* Number of parallel executions

RCS allows a fair comparison across architectures by estimating the classical computational power of each given sampling task.

- *Useful for calibration of NISQ devices.* Critical issues such as cross-talk [3, 4, 7, 20] only come up when scaling multi-qubit computations. XEB with RCS allows for calibration on different sets of qubits at different depths.

Other techniques for benchmarking NISQ devices, such as randomized benchmarking [41–43], cycle benchmarking [44] or preparing entangled GHZ states [5] are restricted to non-universal gate sets and easy to simulate quantum circuits. This is an advantage for extracting circuit fidelities of non-universal gate sets, but does not measure computational power.

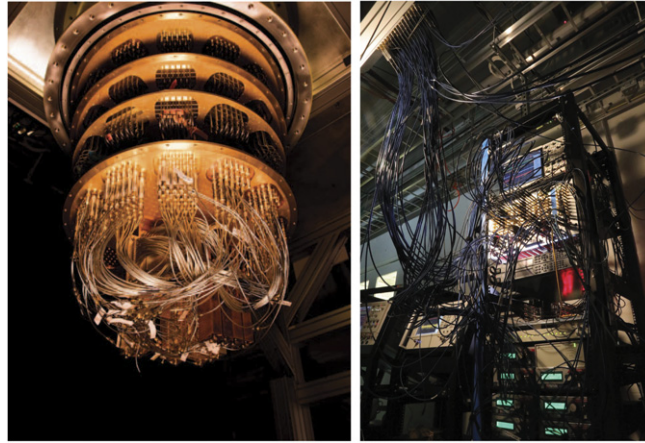


**Figure 2.** A side by side view of a dilution refrigerator and electronic racks for Google's quantum computer.

### 1.3. Energy advantages of quantum computing

The largest casualty as we approach the end of Moore's law has been the energy efficiency gains due to Dennard scaling, also known as Koomey's law. Today's HPC data centers are usually built within the constraints of available energy supplies, rather than the constraints in hardware costs. For example, the Summit HPC system at Oak Ridge National Laboratory has a total power capacity of 14 MW available to achieve a design specification of 200 Pflop/s double-precision performance. To scale such a system by  $10\times$  would require 140 MW of power, which would be prohibitively expensive. Quantum computers on the other hand have the opportunity to drastically reduce power consumption [45, 46].

To compare the energy consumption needed for a classical computation to the corresponding needs of a quantum computation, it is important to understand the sources of energy consumption for quantum computers. For superconducting quantum computers such as Google's (figure 2), the main sources of energy consumption are:

- Dilution refrigerator—because quantum computers operate at around the 15 mK range, a large dilution refrigerator that typically consumes  $\sim 10$  kW is necessary.
- Electronic racks—these typically consume around 5 kW of power. They consist of oscilloscopes, microwave electronics, analog–digital converters, and clocks.

Therefore a typical quantum computer will consume approximately  $\sim 15$  kW of power for a single QPU of 53 qubits. Even as qubit systems scale up, this amount is unlikely to significantly grow. The main reasons are: dilution refrigerators are not expected to scale up; the power for the microwave electronics on a per-qubit basis will decrease as quantum chips scale in the number of qubits. The last component needed to perform a fair comparison between classical and quantum computing is the rate at which quantum computers can execute a circuit. In the case of superconducting qubits, the circuit execution rate is approximately 10–100 kHz.

For classical computers, different architectures can result in different energy consumption rates. In this paper, we compare the consumption of NASA's supercomputer Electra and ORNL's supercomputer Summit. On ORNL's Summit, each node consumes around 2.4 kW of energy and consists of 2 IBM Power9 CPUs and 6 NVIDIA V100 GPUs, with a total of 4608 nodes (1.8 kW per node is consumed by 6 NVIDIA Volta GPUs). On NASA's Electra supercomputer, each of the 2304 40-core Skylake nodes consumes about 0.52 kW, and each of the 1152 28-core Broadwell nodes consumes about 0.38 kW.

## 2. Current state-of-the-art

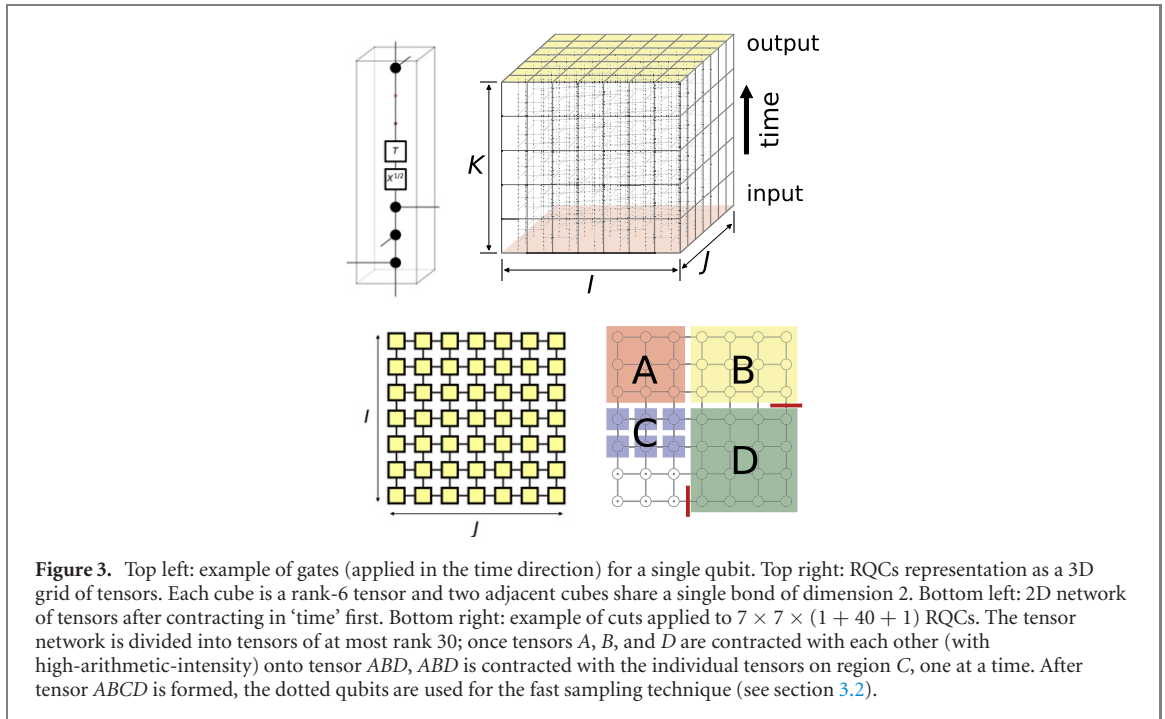
With the advent of NISQ devices, different classes of classical simulators have blossomed to tackle the demanding problem of simulating large RQCs. To date, classical simulators of RQCs can be classified into three main classes (plus a fourth category of 'hybrid' algorithms):

- *Direct evolution of the quantum state.* This approach consists in the sequential application of quantum gates to the full representation of an  $n$ -qubit state. While this method does not have any limitation in terms of gates and topology of RQCs, the memory required to store the full quantum state quickly explodes as  $2^n$ , and taking into account the non-negligible overhead given by the node-to-node communication to update the full quantum state. Thus, this approach becomes impractical for the



simulation and benchmark of NISQ devices with  $\sim 50$  qubits. Beyond  $\sim 40$  qubits it already requires fast internode connectivity [21, 23, 24, 27, 33].

- *Perturbation of stabilizer circuits.* It is known that stabilizer circuits, i.e. quantum circuits made exclusively of Clifford gates, can be efficiently simulated and sampled on classical computers [47]. An intriguing idea consists in representing RQCs as a linear combination of different stabilizer circuits [48–50]. Therefore, the computational complexity to simulate RQCs becomes proportional to the number  $\chi$  of stabilizer circuits required to represent them. Unfortunately,  $\chi$  doubles every time a non-Clifford gate (for instance, a  $\frac{\pi}{8}$  rotation) is used. Furthermore, the number of non-Clifford gates grows quickly with the depth of RQCs [18] and, in general, much faster than the number of qubits. Consequently, stabilizer circuits are not suitable to benchmark NISQ devices using RQCs.
- *Tensor network contractions.* The main idea of this approach is based on the fact that any given quantum circuit can always be represented as a tensor network, where one-qubit gates are rank-2 tensors (tensors of 2 indexes with dimension 2 each), two-qubit gates are rank-4 tensors (tensors of 4 indexes with dimension 2 each), and in general  $n$ -qubit gates are rank- $2n$  tensors [51, 52] (this approach should not be confused with another application of tensor network theory to quantum circuit simulations where tensor networks are used for wave-function compression [53]). In general, the computational and memory cost for contracting such networks is (at least) exponential with the number of open indexes (corresponding to the input state and output state, respectively). Therefore, for large enough circuits, the network contraction is impractical. Nonetheless, once the input and output states are specified through rank-1 Kronecker projectors, the computational complexity drastically reduces. More precisely, the computational and memory costs are dominated by the largest tensor during the contraction [51]. The size of the largest contraction can be estimated by computing the treewidth of the underlying tensor network's line graph which is, for most of the NISQ devices, proportional to the depth of the RQCs. This representation of quantum circuits gives rise to an efficient simulation technique to simulate RQCs for XEB. Among the most relevant tensor-based simulators, it is worth to mention the following:
  - \* *Undirected graphical model.* An approach based on algorithms designed for undirected graphical models, closely related to tensor network contractions, was introduced in [54]. Later, the Alibaba group used the undirected graphical representation of RQCs to take advantage of underlying weaknesses of the design [30]. More precisely, by carefully projecting the state of a few nodes in the graph, the Alibaba group was able to reduce the computational complexity to simulate large RQCs. However, it is important to stress that [30] reports the computational cost to simulate a class of RQCs which is much easier to simulate than the class of RQCs reported in reference [18]. Indeed, Chen *et al* fail to include the final layer of Hadamard gates in their RQCs and use more T gates in detriment of non-diagonal gates at the beginning of the circuit. For these reasons, we estimate that such a circuit class is about  $1000\times$  easier to simulate than the RQCs available in [55], as discussed in reference [32]. The latter are the circuits simulated in this submission, as well as in [31, 32]. See appendix A for more details about this simulator.
  - \* *Quantum teleportation-inspired algorithms.* Recently, Chen *et al* have proposed a related approach for classical simulation of RQCs inspired by quantum teleportation [56]. Such approach allows to 'swap' space and time to take advantage of low-depth quantum circuits (equivalent to a Wick rotation in the imaginary time direction). While the approach is interesting *per se*, the computational performance is lower than that one achieved by qFlex [32].
- *Hybrid algorithms.* Several works have explored algorithms based on splitting grids of qubits in smaller sub-circuits, which are then independently simulated [28, 31]. As an example, every time a CZ-gate crosses between sub-circuits, the number of independent circuits to simulate is duplicated. Therefore, the computational cost is exponential in the number of entangling gates in a cut. MFIB [31] also introduced a technique to 'match' the target fidelity  $f$  of the NISQ device, which actually reduces the classical computation cost by a factor  $f$ . By matching the fidelity of a realistic quantum hardware ( $f = 0.51\%$ ), MFIB was able to simulate  $7 \times 7$  and  $7 \times 8$  grids with depth  $1 + 40 + 1$  by numerically computing  $10^6$  amplitudes in respectively 582 000 and 1407 000 core hours on Google Cloud. However, MFIB becomes less efficient than qFlex for grids beyond  $8 \times 8$  qubits because of memory requirements. In principle, one could mitigate the memory requirements by either using distributed memory protocols like MPI, or by partitioning the RQCs in more sub-circuits. Nevertheless, this has been impractical so far. Moreover, the low arithmetic intensity intrinsic to this method (which relies on the direct evolution of subcircuits) makes it not scalable for flop-oriented heterogeneous architectures like Summit.



### 2.1. qFlex

In 2018, NASA and Google implemented a circuit simulator—qFlex—to compute amplitudes of arbitrary bitstrings and ran it on NASA’s Electra and Pleiades supercomputers [32]. qFlex novel algorithmic design emphasizes communication avoiding and minimization of memory footprint, and it can also be reconfigured to optimize for local memory bandwidth. The computational resources required by qFlex for simulating RCS are proportional to the fidelity of the NISQ device [31, 32]. qFlex provides a fast, flexible and scalable approach to simulate RCS on CPUs (see section 3). In this work, qFlex has been redesigned and reimplemented in collaboration with the Oak Ridge National Laboratory in order to be able to utilize the GPU-accelerated Summit HPC architecture efficiently (see section 3). The computational results presented here, achieving more than 90% of peak performance efficiency and 68% sustained performance efficiency on the world’s most powerful classical computer, define the frontier for quantum computing to declare quantum supremacy. Moreover, given configurability of qFlex as a function of RAM and desired arithmetic intensity, it can be used to benchmark not only NISQ computers, but also classical high-end parallel computers.

## 3. Innovation realized

qFlex is a flexible RQC simulator based on an innovative tensor contraction algorithm for classically simulating quantum circuits that were beyond the reach of previous approaches [32]. More precisely, qFlex is by design optimized to simulate the generic (worst) case RQCs implemented on real hardware, which establish the baseline for the applications of near-term quantum computers. Moreover, qFlex is agnostic with respect to the randomness in the choice of single-qubit gates of the RQCs. Therefore, it presents no fluctuations in performance from one circuit to another in a given ensemble.

For the sake of simplicity, from now on we will focus on planar NISQ devices where qubits are positioned on a grid, with the only entangling gates being CZ gates between two adjacent qubits. As RQCs, we use the prescription described in references [18, 55], which has been shown to be hard to simulate.

Unlike other approaches, the first step of the qFlex algorithm consists of contracting the RQC tensor network in the ‘time’ direction first. This step allows us to reduce the RQC to a regular 2D grid of tensors that are then contracted to produce a single quantum amplitude bitstring (see figure 3). The regularity of the resulting tensors is highly advantageous for exploiting modern classical computer hardware architectures characterized by multi-level cache systems, large vector lengths and high level of parallelism, which requires high arithmetic intensity. The chosen order of tensor contractions is extremely important for minimization of the dimension of the largest tensor during the contraction.

In addition, qFlex expands on a technique introduced in [28–31], which is based on systematic tensor slicing via fine-grained ‘cuts’ that enable us to judiciously balance memory requirements with the number of concurrent computations. Furthermore, by computing an appropriate fraction of ‘paths’, it is possible to control the ‘fidelity’ of the simulated RCS, and therefore to ‘mimic’ the sampling of NISQ devices. Our simulator can produce a sample of  $M$  bitstrings with a target fidelity  $f$  at the same computational cost as to compute  $f \cdot M$  noiseless amplitudes. More importantly, the use of systematic tensor slicing in our tensor contraction algorithm results in complete avoidance of communication between MPI processes, thus making our simulator embarrassingly scalable by design. The number of tensor ‘cuts’ can be properly tuned to fit each independent computation into a single node. Therefore, all the computations required are run in parallel with *no communication* between compute nodes. This is an important design choice that allowed us to avoid the communication bottleneck that would otherwise highly degrade the performance of qFlex, in particular when GPUs are used.

Finally, compared to other approaches, qFlex is the most versatile and scalable simulator of large RCS. In our recent paper [32], qFlex has been used to benchmark the Google Bristlecone QPU of 72-qubits. To date, our Bristlecone simulations are the largest numerical computation in terms of sustained Pflop/s and the number of nodes utilized ever run on NASA Ames supercomputers, reaching a peak of 20 Pflop/s (single precision), corresponding to an efficiency of 64% of the Pleiades and Electra supercomputers. On Summit, we were able to achieve a sustained performance of 281 Pflop/s (single precision) over the entire supercomputer, which corresponds to an efficiency of 68%, as well as a peak performance of 92%, simulating circuits of 49 and 121 qubits on a square grid.

To achieve the performance reported here, we have combined several innovations. Some of them have appeared previously in the literature, as is explained in detail in their corresponding sections (see reference [32] for more details on the techniques and methods used here).

### 3.1. Systematic tensor slicing technique: communication avoiding and memory footprint reduction

For RCS with sufficient depth, the contraction of the corresponding 2D grid of tensors will inevitably lead to the creation of a temporary tensor whose size exceeds the total amount of memory available in a single node. For instance, for a  $7 \times 7$  RQC of depth  $(1 + 40 + 1)$ , the memory footprint exceeds the terabytes of memory. To limit the memory footprint and allow the possibility to contract RQCs on single nodes without communication, we further expand and optimize the technique of using ‘cuts’ [28–31].

Given a tensor network with  $n$  tensors and a set of indexes to contract  $\{i_l\}_{l=1,\dots,n}$ ,  $\sum_{i_1,i_2,\dots} T^1 T^2 \dots T^n$ , we define a cut over index  $i_k$  as the decomposition of the contraction into  $\sum_{i_k} \left( \sum_{\{i_l\}_{l=1,\dots,\{i_k\}}} T^1 T^2 \dots T^n \right)$ . This results in the contraction of up to  $\dim(i_k)$  many tensor networks of lower complexity, namely those covering all slices over index  $i_k$  of the tensors involving that index. The resulting tensor networks can be contracted independently, which results in a computation that is embarrassingly parallelizable. It is possible to make more than one cut on a tensor network, in which case  $i_k$  refers to a multi-index, as well as to adaptively choose the size of the slices. The contribution to the final sum of each of the contractions (each of the slices over the multi-index cut) is a ‘path’, and the final value of the contraction is the sum of all path contributions.

Figure 3 depicts the cut we used for RQCs of size  $7 \times 7$  and depth  $(1 + 40 + 1)$ . The chosen cut allows us to reduce the amount of memory to fit six contractions on each Summit node (one FPR each GPU). Moreover, as explained in the next sections, such cuts will greatly improve the sampling of amplitudes for a given RQC.

### 3.2. Fast sampling technique

Sampling is a critical feature of random circuit sampling (RCS) and, therefore, it must be optimized to reduce the time-to-solution. To this end, we use a *frugal rejection sampling* which is known to have a low overhead for RCS [31]. In addition, as explained in reference [32], a faster sampling can be achieved by recycling most of the large contraction for a given amplitude calculation. More precisely, if different tensors  $A_1(x_1), \dots, A_k(x_1)$  and  $C(x_2)$  must be contracted to get the amplitude of bitstring  $x = x_1 \cup x_2$ , our fast sampling technique first contracts all  $A_i(x_1)$  tensors (for a given  $x_1$ ) to get a tensor  $B$ . Then,  $B$  is recycled and contracted to  $C(x_2)$  for many different  $x_2$ . Since the most computationally demanding part is the calculation of  $B$ , many amplitudes  $x = x_1 \cup x_2$  can be computed with different  $x_2$  (but the same  $x_1$ ). Since RQCs are extremely chaotic, arbitrary close bitstrings are uncorrelated [18]. These amplitudes are used to perform the frugal rejection sampling of one single output bitstring in the output sample, and the computation is restarted with a new random  $x_1$  to output the next bitstring. For deep enough RQCs and by carefully choosing the size of  $x_2$ , one can reduce the sampling time by an order of magnitude, as shown in [32].



### 3.3. Noisy simulation

Given the noisy nature of NISQ devices, simulating noisy RCS is of utmost importance. Intuitively, one would expect that noisier RCS would be easier to simulate. Indeed, as shown in reference [31], independent tensor contractions to compute a single amplitude can be seen as orthogonal ‘Feynman paths’ (or simply ‘paths’). Since RQCs are very chaotic and Feynman paths typically contribute equally to the final amplitude, computing only a fraction  $f$  of paths is equivalent to computing noisy amplitudes of fidelity  $f$ . The computational cost for a typical target fidelity of 0.5% for NISQ devices is therefore reduced by a factor of 200 [31, 32].

While computing only a fraction of paths allows for a speedup in the simulation of noisy devices, computing fewer amplitudes with higher fidelity is an alternative method to achieve a similar speedup, as we introduced in reference [32]. In particular, computing a fraction  $f$  of perfect fidelity amplitudes from a target amplitude set lets us simulate RCS with fidelity  $f$ . In general, the fraction of amplitudes computed times their fidelity equals the fidelity of the simulated sampling.

### 3.4. Optimization of the tensor contraction order for optimal time-to-solution

The optimization of the number and position of the cuts and the subsequent tensor contraction ordering is fundamental for minimizing the total flop count and the time-to-solution in evaluating a given tensor network and to simulate sampling. Note that on modern flop-oriented computer architectures the minimal flop count does not necessarily guarantee the minimal time-to-solution, making the optimization problem even more complicated. Indeed, different tensor contraction orderings can result in performances that differ by orders of magnitude. In general, finding the optimal cuts and tensor contraction order is an NP-hard problem (closely related to the tree-decomposition problem [51]). However, for planar or quasi-planar tensor network architectures produced by most of the NISQ devices, such tensor cuts can be found by carefully splitting the circuits into pieces that minimize the shared boundary interface; furthermore, we find that choosing a contraction ordering that prioritizes a few large, high arithmetic intensity contractions over many smaller, low arithmetic intensity contractions, often provides large speedups, and therefore better time-to-solution.

### 3.5. Out-of-core asynchronous execution of tensor contractions on GPU

The novel tensor slicing technique used by the qFlex algorithm removes the necessity of the inter-process MPI communication and controls the memory footprint per node, thus paving the way to scalability. In order to achieve high utilization of the hardware on a heterogeneous Summit node, we implemented an out-of-core GPU tensor contraction algorithm in the TAL-SH library [57], which serves as a computational backend in qFlex. The TAL-SH library is a numerical tensor algebra library capable of executing basic tensor algebra operations, most importantly tensor contraction, on multicore CPU and NVIDIA GPU hardware. The key features of the TAL-SH library that allowed us to achieve high-performance on GPU-accelerated node architectures are: (a) fast heterogeneous memory management; (b) fully asynchronous execution of tensor operations on GPU; (c) fast tensor transpose algorithm; (d) out-of-core algorithm for executing large tensor contractions on GPU (for tensor contractions that do not fit into individual GPU memory).

The fast CPU/GPU memory management, and in general fast resource management, is a necessary prerequisite for achieving high level of asynchronism in executing computations on CPU and GPU. TAL-SH provides custom memory allocators for host and device memory. These memory allocators use pre-allocated memory buffers acquired during library initialization. Within such a buffer, each memory allocator implements a simplified version of the ‘buddy’ memory allocator used in Linux. Since the memory allocation/deallocation occurs inside pre-allocated memory buffers, it is fast and it is free from highly unwanted side effects associated with regular CUDA malloc/free, for example serialization of asynchronous CUDA streams.

All basic tensor operations provided by the TAL-SH library can be executed asynchronously with respect to the CPU Host on any GPU device available on the node. The execution of a tensor operation consists of two phases: (a) scheduling (either successful or unsuccessful, to be re-tried later); (b) checking for completion, either testing for completion or waiting for completion (each scheduled tensor operation is a TAL-SH task with its associated TAL-SH task handle that is used for completion checking). All necessary resources are acquired during the scheduling phase, thus ensuring an uninterrupted progress of the tensor operation on a GPU accelerator via a CUDA stream. The tensor operation scheduling phase includes scheduling the necessary data transfers between different memory spaces, which are executed asynchronously as well. The completion checking step also includes consistency control for images of the same tensor in different memory spaces. All these are automated by TAL-SH.

The tensor contraction operation in TAL-SH is implemented by the general transpose–transpose–GEMM–transpose (TTGT) algorithm, with an optimized GPU tensor transpose operation [58] (see also reference [59]). In the TTGT algorithm, the tensor contraction operation is converted to the matrix–matrix multiplication via permuting tensor indexes. The performance overhead associated with the tensor transpose steps can be as low as few percent, or even lower for highly arithmetically intensive tensor contractions, when using the optimized implementation. Also, all required host-to-device and device-to-host data transfers are asynchronous, and they overlap with kernels execution in other concurrent CUDA streams, thus minimizing the overhead associated with CPU–GPU data transfers. Additionally, TAL-SH provides an automated tensor image consistency checking mechanism, enabling tensor presence on multiple devices with transparent data consistency control (tensor image is a copy of the tensor on some device).

In this work, we used the regular complex FP32 CGEMM implementation provided by the cuBLAS library, without tensor core acceleration. The possibility of reducing the input precision to FP16 in order to use Volta’s tensor cores is strongly conditioned by the precision needed for simulating large quantum circuits. The average squared output amplitude of a quantum circuit of  $n$  qubits is  $1/2^n$ , which for  $n = 49$  (simulated in this work) is of the order of  $10^{-15}$  and for  $n = 121$  (also simulated here) is of the order of  $10^{-37}$ . We avoid the possibility of underflowing single precision by normalizing the input tensors, and renormalizing them back at the end of the computation.

Finally, an important extension to the basic TAL-SH functionality, which was the key to achieving high performance in this work, is the out-of-core algorithm for executing large tensor contractions on GPU, that is, for executing tensor contractions which do not fit into individual GPU memory. Although the Summit node has IBM AC922 Power9-Volta architecture with unified CPU–GPU coherent memory efficiently synchronized via NVLink, we did not rely on the unified memory abstraction provided by the CUDA framework for two reasons. First, although the hardware assisted memory page migration is very efficient on this architecture, we believe that the explicitly managed heterogeneous memory and data transfers deliver higher performance for tensor contractions (this is an indirect conclusion based on the performance of similar algorithms on Summit). Second, the TAL-SH library prioritizes performance portability among other things, that is, it is meant to deliver high performance on other accelerated HPC systems as well, many of which do not have hardware-assisted coherence mechanism between CPU and GPU.

The out-of-core tensor contraction algorithm implemented in TAL-SH is based on recursive decomposition of a tensor operation (tensor contraction in this case) into smaller tensor operations (tensor contractions) operating on slices of the original tensors, following the general philosophy presented in reference [60]. During each decomposition step, the largest tensor dimension associated with the largest matrix dimension in the TTGT algorithm is split in half (in TTGT algorithm multiple tensor dimensions are combined into matrix dimensions, thus matricizing the tensors). This ensures maximization of arithmetic intensity of individual derived tensor contractions, which is important for achieving high performance on modern flop-oriented computer architectures, like the NVIDIA Volta GPU architecture employed in this work (arithmetic intensity is the flop-to-byte ratio of a given operation). The recursive decomposition is repeated until all derived tensor operations fit within available GPU resources. Then the final list of derived tensor operations is executed by TAL-SH using a pipelined algorithm in which multiple tensor operations are progressed concurrently, thus overlapping CPU and GPU elementary execution steps. In general, TAL-SH allows tuning of the number of concurrently progressed tensor operations, but in this work we restricted it to 2. Each tensor operation has five stages of progress:

- (a) Resource acquisition on the execution device (GPU);
- (b) Loading input tensor slices on host (multithreaded);
- (c) Asynchronous execution on GPU: fast additional resource acquisition/release, asynchronous data transfers, asynchronous tensor transposes, asynchronous GEMM;
- (d) Accumulating the output tensor slice on host (multithreaded);
- (e) Resource release on the execution device (GPU).

The pipelined progressing algorithm is driven by a single CPU thread and is based on the ‘asynchronous yield’ approach, that is, each active (concurrent) tensor operation proceeds through its consecutive synchronous stages uninterrupted (unless there is a shortage in available resources, in which case it is interrupted), but it ‘yields’ to the next concurrent tensor operation once an asynchronous stage starts. The asynchronous GPU execution step, mediated by the CUDA runtime library, involves asynchronous host-to-device and device-to-host data transfers, asynchronous (optimized) tensor transpose kernels and asynchronous (default) CGEMM cuBLAS calls. Since each NVIDIA Volta GPU has multiple physical data transfer engines, all incoming and outgoing data transfers are overlapped with the CUDA kernels execution

in different CUDA streams, thus almost completely removing CPU–GPU data transfer overhead. Overall, this algorithm, combined with fast tensor transpose and efficient cuBLAS GEMM implementation, results in highly efficient execution of large tensor contractions on GPU, as demonstrated by our results (up to 96% of Volta’s theoretical flop/s peak).

#### 4. How performance was measured

We used an analytical approach to measuring the number of floating point operations performed by our algorithm. Our computational workload consists of a series of tensor contractions operating on dense tensors of rank 1 to 10. Thus, the total number of flops executed by an MPI process is the sum of the flop counts of each individual tensor contraction executed by that MPI process. Each individual tensor contraction has a well defined flop count:

$$F = 8\sqrt{v_0 \cdot v_1 \cdot v_2} \quad (1)$$

where  $v_0, v_1, v_2$  are the volumes of the tensors participating in the tensor contraction (volume is the number of tensor elements in a tensor), and the factor of 8 shows up due to the use of the complex multiply-add operation (4 real multiplications plus 4 real additions). All tensors used in our simulations are of complex single precision (complex FP32), SP.

For the timing of the simulations, we do not include job launching, `MPI_Init()`, nor the initialization of the TAL-SH library on each MPI process, as well as the final time taken to write the results to file by the master MPI process (scheduler). In order to do so, the two timings are reported after two `MPI_Barrier()` synchronization calls.

Based on the analytical flop count calculation, we have computed multiple performance metrics in this work. The average SP flop/s count,  $C_A$ , is computed by dividing the total flop count of our simulation by its execution time. The peak SP flop/s count,  $C_P$ , is computed by dividing the total flop count of the largest tensor contraction by the sum of its execution times on each node, times the number of nodes. Additionally, we have computed the energy efficiency of the Summit hardware with respect to our simulation. The average flop/s/watt value,  $E_A$ , is computed by dividing the total flop count of our simulation by the total energy consumed by Summit during the simulation. This energy consumption value is actually the upper bound because it includes all components of Summit, some of which, like disk storage, were not actively used by our simulation. The Summit HPC system at Oak Ridge National Laboratory has a total power capacity of 14 MW available to achieve a design specification of slightly more than 200 Pflop/s peak double-precision performance, and more than 400 Pflop/s single-precision performance. This energy powers 4608 GPU-enabled compute nodes. Each Summit node contains 2 Power9 CPU, 6 NVIDIA Volta V100 GPUs, 512 GB of DDR4 RAM, 16 GB of HBM2 on-chip GPU memory in each GPU, 1.6 TB of non-volatile NVMe storage, and 2 physical network interface cards, with a total power cap of approximately 2400 W, of which up to 1800 W are consumed by the 6 NVIDIA Volta GPUs.

#### 5. Performance results

We have simulated RCS on two large hard RQCs running on either half or the entire Summit supercomputer. Both circuits belong to the class of revised, worst-case circuits on planar graphs (no design weaknesses exploited) [31] and can be found in [55] (`inst_7 × 7_41_0.txt` and `inst_11 × 11_25_0.txt`). See table 1 for a summary of our performance results.

##### 5.1. GPU results and peak performance

Most of the simulation time is spent in arithmetically intensive, out-of-core contractions of large tensors (with volumes as large as  $v_0 = v_1 = v_2 = 2^{30}$ ) that do not necessarily fit in the GPU memory. On these contractions, we achieve a performance efficiency of over 90% with respect to the theoretical single-precision peak of 15 Tflop/s for the NVIDIA Volta V100 GPUs, and this efficiency goes as high as 96%. For this reason, we compute our peak performance as the average performance of these largest tensor contractions times the number of GPUs corresponding to the number of nodes used in each simulation. We therefore achieve a peak performance of 92% (381 Pflop/s when running on 100% of Summit) in the  $7 \times 7 \times (1 + 40 + 1)$  simulation, and 90% (367 Pflop/s when running on 99% of Summit) in the  $11 \times 11 \times (1 + 24 + 1)$  simulation.

##### 5.2. Sustained performance

While we successfully slice (‘cut’) the tensors in our circuits and contract them in an ordering that leaves most of the computation to large arithmetically intensive tensor contractions, it is inevitable to deal with a

**Table 1.** Performance of the simulation of our three runs on Summit. For the  $7 \times 7 \times (1 + 40 + 1)$  circuit we computed 1.01 million amplitudes with fidelity  $6/1024 \approx 0.5\%$  on each run, while for the  $11 \times 11 \times (1 + 24 + 1)$  circuit we computed 325 000 amplitudes of fidelity  $1/64$ , which equivalently allows us to sample with fidelity  $f \approx 0.5\%$  (see section 3.3). The performance is compared against the theoretical peak performance, where a maximum of single-precision 15 Tflop/s is considered for each NVIDIA Volta GPU, and then extrapolated to the number of nodes used (with 6 GPUs per node). The results show a stable sustained performance between the simulation of the  $7 \times 7 \times (1 + 40 + 1)$  circuit on 2300 (50% of Summit) and 4600 nodes (100% of Summit). The (average) power consumption reported was measured for the entire Summit, and is therefore not considered when running on half of the nodes.

Circuit size	Nodes used	Runtime (h)	PFlop/s		Efficiency (%)		Power (MW)	Energy cost (MWh)	PFlop ( $s^{-1}MW^{-1}$ )
			Peak	Sust.	Peak	Sust.			
$7 \times 7 \times (1 + 40 + 1)$	2300	4.84	191	142	92.0	68.5	—	—	—
$7 \times 7 \times (1 + 40 + 1)$	4600	2.44	381	281	92.1	68.0	8.075	21.1	34.8
$11 \times 11 \times (1 + 24 + 1)$	4550	0.278	368	261	89.8	63.7	7.3	2.32	35.8

non-negligible number of less arithmetically intensive tensor contractions, which achieve a suboptimal performance. Averaged over the entire simulation time, we reach a sustained performance efficiency of about 68% (281 Pflop/s on 100% of Summit) for the  $7 \times 7 \times (1 + 40 + 1)$  simulation, and about 64% (261 Pflop/s on 99% of Summit) for the  $11 \times 11 \times (1 + 24 + 1)$  simulation. Compared to our previous simulations of random quantum circuits ran on the CPU-only Pleiades/Electra HPC systems at NASA [32], the GPU-accelerated Summit node (2 CPU + 6 GPU) delivers about 45.6 speed-up in running qFlex as compared to the performance of the averaged Pleiades/Electra dual-CPU node (Pleiades/Electra HPC systems consist of dual-socket CPU nodes with different families of Intel CPUs which we average over). The actual single-precision performance delivered by the averaged Pleiades/Electra node is 1.34 Tflop/s/node, compared to 61.09 Tflop/s/node sustained by the heterogeneous Summit node. The speed-up is even higher for the peak performance achieved on both systems.

### 5.3. Scaling

Due to the communication-avoiding design of our algorithm, the impact of communication on scaling is negligible, and therefore the performance is stable as a function of the number of nodes used, demonstrating an excellent strong scaling (see table 1).

### 5.4. Energy consumption

We report the energy consumed by Summit in our full scale simulations. We achieve a rate of 34.8 Pflop/s/MW for the  $7 \times 7 \times (1 + 40 + 1)$  simulation, and 35.8 Pflop/s/MW for the  $11 \times 11 \times (1 + 24 + 1)$  simulation. Note that the power consumed should be taken as an upper bound, since it takes into account the consumption of the entire machine, including components that were not used in the simulations. Furthermore, we report the energy consumed by the entire job, including job launch and initialization of the TAL-SH library, which again slightly lifts the upper bound; this might be part of the reason for obtaining a slightly larger flop per energy rate on the shorter simulation ( $11 \times 11 \times (1 + 24 + 1)$ ), see figure 4), where the actual computing time is smaller in relative terms.

## 6. Implications and conclusions

As we explore technologies beyond Moore's law, and in particular as we enter the NISQ era with quantum devices that surpass classical capabilities [7], it is important to understand the potential advantages of quantum computing both in terms of time-to-solution and energy consumption. The research presented here also provides a comparison of different classical computing architectures, comparing random circuit sampling implementations on both CPU and GPU based supercomputers (see table 2).

In conclusion, the implications of the proposed research are the following:

- *Establishes minimum hardware requirements for quantum computers to exceed available classical computation.* qFlex is able to calculate the required fidelity, number of qubits, and gate depth required for a quantum computer to exceed the computational ability of the most powerful available supercomputer for at least one well defined computational task: RCS. The demonstration of quantum computational supremacy of reference [7] well surpasses this threshold.
- *Objectively compares quantum computers in terms of computational capability.* Different architectures (e.g. ion traps vs superconducting qubits) vary in:
  - \* Number of qubits
  - \* Types of gates

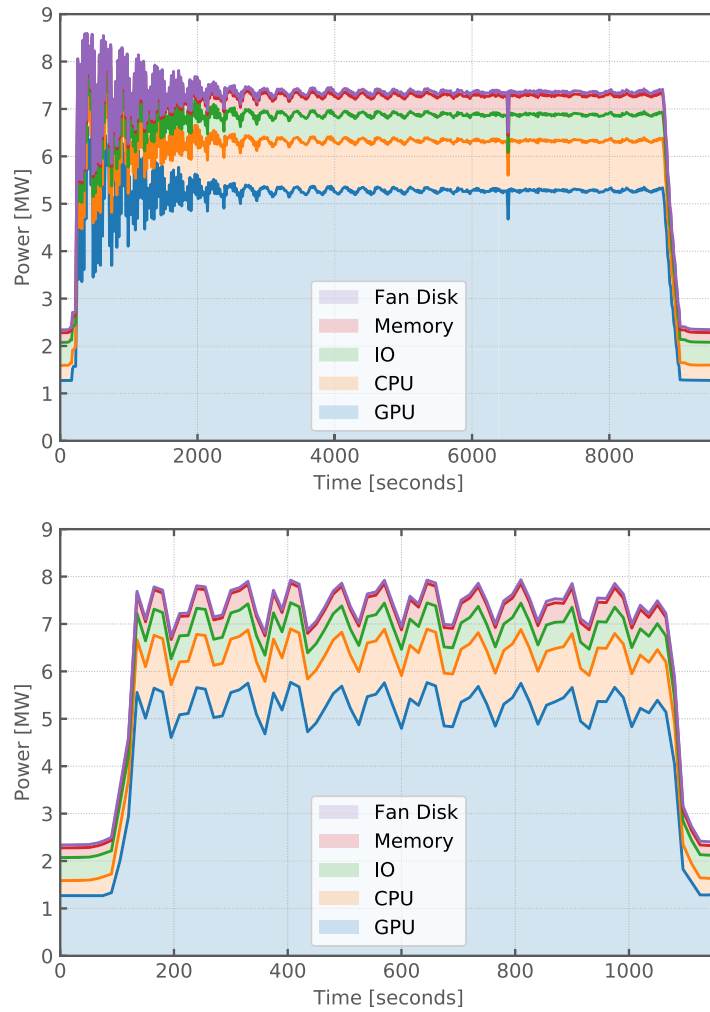


**Figure 4.** Power consumption of Summit, at a given time, during our simulations. Note that most of the power is consumed by the GPUs. (Top)  $7 \times 7 \times (1 + 40 + 1)$  over 4600 nodes. (Bottom)  $11 \times 11 \times (1 + 24 + 1)$  over 4550 nodes.

- \* Fidelity
- \* Connectivity
- \* Number of qubits per multi-qubit operation
- \* Number of parallel executions

RCS allows comparisons across different qubit architectures estimating the equivalent amount of classical computation with commonly used metrics.

- *Establishes a multi-qubit benchmark for non-Clifford gates.* Prior to XEB, there was no benchmarking proposal to measure multiqubit fidelity for universal (non-Clifford) quantum gate sets. qFlex enables XEB on a large number of qubits and large circuit depths by efficiently using classical computing resources. XEB allows quantum hardware vendors to calibrate their NISQ devices.
- *Objectively compares classical computers for simulating large quantum many-body systems.* Using RCS as a benchmark for classical computers, one can compare how different classical computers perform simulation of large quantum many-body systems across different classical computational architectures. In this paper, we specifically compare NASA's Electra supercomputer, which is primarily powered by Intel Skylake CPUs, with ORNL's Summit supercomputer, which is primarily powered by NVIDIA Volta GPUs.
- *Objectively compares computer energy consumption requirements across a variety of quantum and classical architectures for one specific computational task.* We estimated the energy cost to produce a sample of  $10^6$  bistrings for 2 different circuits across classical CPU, GPU, and superconducting quantum computer architectures (see table 2). The classical computers would take 96.8 MWh and 21.1 MWh for NASA's Electra and ORNL's Summit, respectively. The factor of almost 5 of improvement of Summit over Electra is due to Summit's GPU architecture. Comparing this to a



**Table 2.** Estimated runtimes and energy cost for the sampling of  $10^6$  amplitudes with fidelity close to 0.5% on NASA Electra, ORNL Summit, and a superconducting NISQ device (QPU). For the QPU, we assume a sampling rate of 10 kHz and a power consumption of 15 kW (see section 1.3). Note that the large improvements on time-to-solution and energy consumption of the QPU as compared to state-of-the-art classical supercomputers do not extrapolate to other applications. However, the ‘hello world’ nature of the sampling problem establishes the baseline for the applicability of quantum computers.

Circuit size	Target fidelity (%)	Runtime (hours)			Energy cost (MWh)		
		Electra	Summit	QPU	Electra	Summit	QPU
$7 \times 7 \times (1 + 40 + 1)$	0.5	59.0	2.44	0.028	96.8	21.1	$4.2 \times 10^{-4}$

superconducting quantum computer with a sampling rate of 10 kHz, a quantum computer would have an additional five orders of magnitude improvement (see table 2). This separation in energy consumption performance is much greater than the time-to-solution performance improvement of 2 orders of magnitude. Furthermore, as the number of qubits grows we expect the separation in energy performance to continue to grow faster than the time-to-solution performance. We emphasize that RCS is a computational task particularly favorable to quantum computers and an advantage is presently not achievable in practice for most other computational problems.

- *Guides near-term quantum algorithm and hardware design.* The simulation capabilities of qFlex can be harnessed for such tasks as verifying that a hardware implementation of an algorithm is behaving as expected, evaluating relative performance of quantum algorithms that could be run on near-term devices, and suggesting hardware architectures most suitable for experimenting with specific quantum algorithms in the near term. The specific capabilities of qFlex are particularly useful for evaluating quantum circuits large enough that the full quantum state cannot be produced but for which qFlex can still compute the probability of individual outputs of interest. In the case of RCS, it suffices to compute the amplitudes of random bistrings to perform rejection sampling in order to produce a sample of bistrings [31, 32]. In other cases, it might be possible to use classical heuristics to determine what probabilities to calculate.

## Acknowledgments

We are grateful for support from NASA Ames Research Center, NASA Advanced Exploration systems (AES) program, and NASA Transformative Aeronautic Concepts Program (TACP), and also for support from AFRL Information Directorate under grant F4HBKC4162G001. TSH acknowledges support from the Department of Energy Office of Science Early Career Research Program. This research used resources of the Oak Ridge Leadership Computing Facility, which is a DOE Office of Science User Facility supported under Contract DE-AC05-00OR22725. We would like to thank Jack Wells, Don Maxwell, and Jim Rogers for their help in making Summit simulations possible and for providing hardware utilization statistics. This manuscript has been authored by UT-Battelle, LLC under Contract No. DE-AC05-00OR22725 with the U.S. Department of Energy. The United States Government retains and the publisher, by accepting the article for publication, acknowledges that the United States Government retains a non-exclusive, paid-up, irrevocable, world-wide license to publish or reproduce the published form of this manuscript, or allow others to do so, for United States Government purposes. The Department of Energy will provide public access to these results of federally sponsored research in accordance with the DOE Public Access Plan. (<http://energy.gov/downloads/doe-public-access-plan>).

## Appendix A. Comparison with variable elimination algorithms

As discussed in section 2, variable elimination algorithms over undirected graphical models can be used to simulate quantum circuits, which has been successfully exploited in references [30, 54, 61]. In this appendix we estimate the computational resources needed by such algorithms to simulate the circuits presented in this work. In our estimates, we make use of the algorithm and benchmarks presented in references [30, 61].

### A1. Algorithm

The main idea is to represent the tensor network (TN) of a quantum circuit as a graph closely related to its line graph: an undirected graphical model. Each vertex in the graph corresponds to a unique index in the TN, and is therefore a binary variable. For each tensor or gate in the TN shared by a set of vertices, edges are added to the graph so that such vertices are connected all-to-all, forming a clique (complete subgraph). By

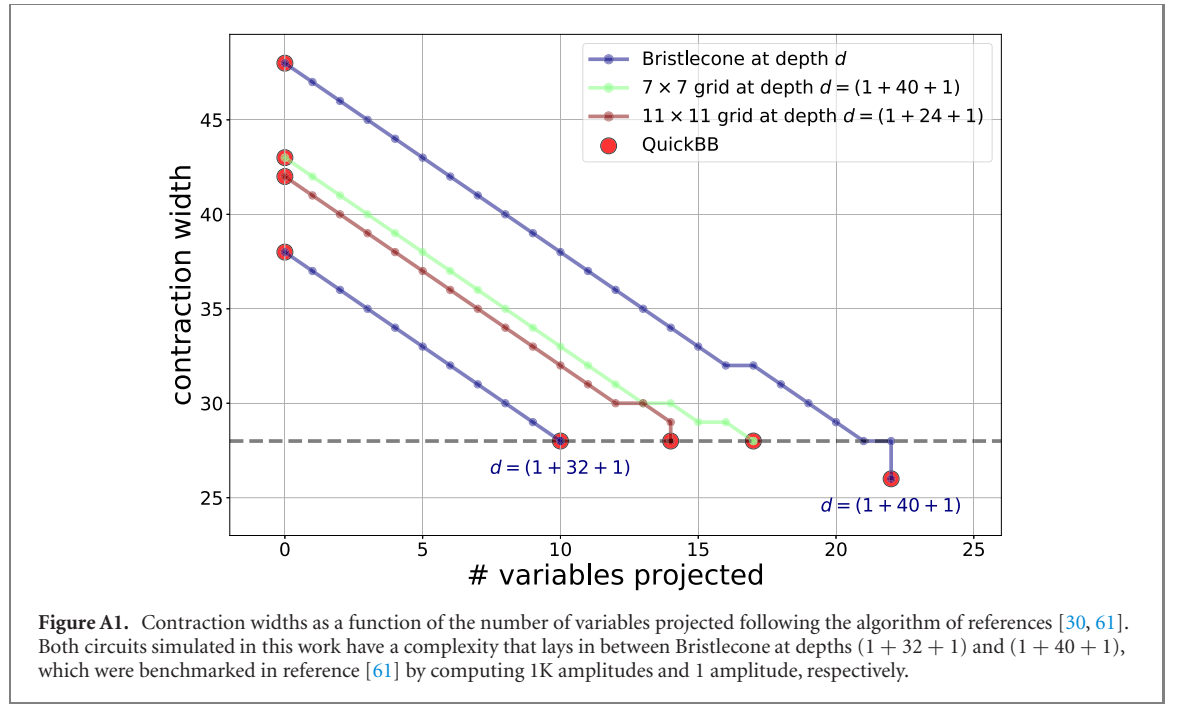
representing TNs this way, one can take advantage of the structure of particular gates and explicitly simplify the problem by obtaining a simpler graph. For example, diagonal two-qubit gates have only two distinct variables (vertices in the graph), unlike general two-qubit gates, which have four; in addition, diagonal one-qubit gates have a single variable, instead of two. This representation is equivalent to TNs if these are allowed to have hyperedges, corresponding to the situation where a vertex belongs to more than two cliques (tensors) simultaneously.

Once the undirected graphical model corresponding to a circuit is built, the contraction is carried out in a similar way as a TN contraction, which is referred to as a variable elimination procedure. We will use the terms contraction and elimination interchangeably. The variable elimination over the entire graph proceeds as follows. First, an elimination ordering is chosen. Each variable being eliminated corresponds to the contraction of an index from a TN perspective, and results in the elimination of the variable from the graph, as well as the subsequent formation of a clique between all cliques which contained the variable prior to its elimination. This way, as the elimination procedure continues, cliques of different sizes are formed; we define the *contraction width* of the ordering as the size of the largest clique formed along the process. The size of the largest tensor formed along the contraction is equal to  $2^{\text{contractionwidth}}$ . At the same time, the time complexity of the elimination of a variable is proportional to  $2^c$ , where  $c$  is the size of the resulting clique, and so the time complexity of the entire elimination process is proportional to  $\sum_i 2^{c_i}$ , where  $i$  labels all variables, and is dominated by the term  $2^{\text{contractionwidth}}$ . Given an undirected graphical model, finding the elimination ordering that minimizes the contraction width is an NP-hard problem; such optimal contraction width is called the *treewidth* (TW) of the graph. There are heuristic algorithms to find suboptimal elimination orderings, as well as computationally intensive algorithms that guarantee optimality, which also provide suboptimal solutions when run for a finite amount of time. Reference [54] introduced the use of QuickBB for finding good elimination orderings for the simulation of quantum circuits.

If the TW of the graph (or its contraction width found, for practical purposes) is so large that the amount of memory needed for the simulation exceeds computational resources, it is still possible to perform the simulation, as introduced in reference [30]. The idea here is that by projecting a single variable of the graph to either one of its two values, the resulting subgraph (which has lost the vertex corresponding to the variable, as well as all edges adjacent to it) might require substantially lower computational resources, at the expense of doubling the number of graphs we have to evaluate or contract. By choosing a careful subset of variables to project, the resulting subgraphs are easy enough to contract, and their evaluations are independent of each other, making the simulation embarrassingly parallelizable. The projection of a number  $p$  of variables leads to the evaluation of  $2^p$  circuits, all of which have decreased their time complexity by some factor common to all, and have possibly also decreased their contraction width. Reference [30] provides a heuristic algorithm to choose this subset of  $p$  variables that works well in practice. First, QuickBB is run over the initial graph for  $S$  seconds in order to find a good elimination ordering. Then, the contraction costs of the subgraphs that would result from the projection of each variable are computed, and the variable that decreases the resulting cost is chosen to be projected. In doing this, the elimination ordering inherited from the previous step is used. The same procedure is greedily carried out  $p$  times. Finally, QuickBB is run over the final graph (where  $p$  variables have been projected) in an attempt to find a potentially better elimination ordering than the one inherited from the first step; this might in some cases not decrease the elimination cost.

## A2. Methodology

In reference [30], this algorithm was used in order to benchmark the simulation of circuits on square grids of qubits. As explained in reference [32] and in section 2, the circuits benchmarked in reference [30] had gate sequences that made them easier to simulate than those of reference [32] and of the present work. In reference [61], the authors used a newer version of their algorithm to simulate circuits on the Bristlecone grid introduced in [32], with substantial speedups. In this appendix, we use these benchmarks in order to estimate the performance of this variable elimination algorithm in the simulation of the circuits benchmarked here, which are defined over rectangular grids. For this estimate, we have implemented the heuristic algorithm of [30] for choosing the subset of variables that are projected. We have run our implementation of this algorithm on the Bristlecone circuits of reference [61] with a value of  $S = 1800$  s (30 min), which we believe decreases the TW of the resulting graphs enough to fit within the memory resources used, as reported by the authors. Then, with the same setting of  $S = 1800$  s, we run the algorithm over the  $7 \times 7 \times (1 + 40 + 1)$  and the  $11 \times 11 \times (1 + 24 + 1)$  circuits presented here. After projecting enough variables so that the memory requirements of the contractions are as low as those found for the Bristlecone circuits (see figure A1 for the resulting contraction widths), we use the following expression to determine



the computation time for the computation of an amplitude:

$$T = D^{-1} \cdot 2^p \cdot (\text{elim. cost after } p \text{ projections}) / n_{\text{cores}}, \quad (2)$$

where  $D$  is a constant factor,  $p$  is the number of variables projected, and  $n_{\text{cores}}$  is the number of cores used in the computation. Constant  $D$  is obtained from the benchmarking data reported in reference [61]: the computation of an amplitude of Bristlecone circuits at depths  $(1 + 32 + 1)$  and  $(1 + 40 + 1)$  took respectively 0.43 s and 580.7 s when using 127 512 CPU cores. In the first case, 10 variables were projected, while 22 were projected in the second. This leads to a value of  $D = 52.7$  MHz and 51.6 MHz, respectively; we choose to use  $D = 52.7$  MHz in our estimates since it leads to slightly lower computation times. Note that the fact that both values of  $D$  are extremely close to each other gives us confidence that the  $S$  value of QuickBB yields indeed results close to those of reference [61].

In order to have meaningful comparisons between both simulators, we assume that a number of CPUs similar to Summit in the number of delivered FLOPs is accessible. For that, note that each of the Intel Xeon 8163 CPUs used in reference [61] has two AVX-512 units that deliver together 160 Gflops @ 2.5 GHz (single precision). Each node has 88 CPU cores (14.08 Tflops) and in total 1449 nodes are used (127 512 cores), for a total theoretical peak of 20.4 Pflops delivered. Each Summit node delivers a peak of 90 Tflops (see section 5.1), and so it corresponds to 6.4 of the CPU nodes considered here. All 1449 nodes are performance-wise equivalent to about 226 Summit nodes, although with about twice the amount of memory per flop: 160 GB per CPU node compared to 512 GB per Summit node. We therefore consider that 4600 Summit nodes (100% of Summit) correspond to  $n_{\text{cores}} = 127\,512 \times 4600 / 226 = 2595\,377$  CPU cores. Such a number of cores would require  $1449 \times 160 \times 4600 / 226 = 4.72$  PB of memory.

### A3. Results

Table A1 shows the estimated runtimes and memory requirements for the simulation of the circuit presented in the current work using the variable elimination simulator of reference [61]. For comparison, we also include the results of qFlex. For the  $7 \times 7 \times (1 + 40 + 1)$  circuit, qFlex is somewhat faster, and requires about half the memory resources. For the  $11 \times 11 \times (1 + 32 + 1)$ , qFlex is about  $3 \times$  faster, halving also the memory requirements.

### A4. Optimistic assumptions on the variable elimination algorithm

In, section A3 we have computed time estimates for the simulation of random circuit sampling of 1M bitstrings at fidelity 0.5%. However, there are two optimistic assumptions on the performance of the variable elimination simulator that we discuss here. First, sampling 1M bitstrings from an RQC with fidelity 0.5% involves the computation of 5000 perfect fidelity *batches* of amplitudes (see figure 3). One of the disadvantages of variable elimination algorithm of references [30, 61] compared to the tensor network techniques described here is its inability to compute batches of amplitudes of correlated bitstrings at the

**Table A1.** Comparison of qFlex with the variable elimination simulator of references [30, 61] (Alibaba). Runtimes for the sampling of 1M bitstrings at fidelity 0.5% are considered. We extrapolate the runtimes reported in [61] to the circuits benchmarked here, as well as to the peak performance of Summit. This implies assuming that the simulator of [61] is implementable on GPUs with similar efficiency as that one achieved on CPUs. Finally, the fact that fast sampling (see section 3.2) is not implemented for variable elimination algorithms is neglected; considering this fact would increase time estimates for this simulator by a factor of between 3 and 10 (see references [31, 32, 56]).

Simulator	Circuit instance	Num. variables projected, $p$	Cost, $\sum_i 2^{q_i}$	Runtime, $T$ (h)	Memory requirements (PB)
Alibaba	Bristlecone $\times (1 + 32 + 1)$	10	$2.82 \times 10^9$	0.0293	4.72
Alibaba	Bristlecone $\times (1 + 40 + 1)$	22	$9.11 \times 10^8$	38.8	4.72
Alibaba	$7 \times 7 \times (1 + 40 + 1)$	17	$2.48 \times 10^9$	3.31	4.72
Alibaba	$11 \times 11 \times (1 + 24 + 1)$	14	$5.04 \times 10^9$	0.838	4.72
qFlex	$7 \times 7 \times (1 + 40 + 1)$	—	—	2.44	2.36
qFlex	$11 \times 11 \times (1 + 24 + 1)$	—	—	0.278	2.36

same cost as a single amplitude (although it might be possible to implement this technique in the future). Accounting for this fact should increase the computation time to sample a bitstring by a multiplicative factor (between 3 and 10, in practice, as shown in references [31, 32, 56]). Second, we assume that a variable elimination algorithm is successfully implemented to run efficiently on GPUs, which is in principle hindered by the low arithmetic intensity of the contraction of variables one at a time; given such an assumption, runtimes for this algorithm on Summit can be estimated. We have made these assumptions in order to give what we consider would be the best possible scenario in which variable elimination algorithms could operate; estimates should be larger by some factors.

## ORCID iDs

Salvatore Mandrà  <https://orcid.org/0000-0002-3908-2694>

## References

- [1] Feynman R P 1982 Simulating physics with computers *Int. J. Theor. Phys.* **21** 467–88
- [2] Feynman R P 1985 Quantum mechanical computers *Optics News* **11** 11–20
- [3] Barends R *et al* 2014 Superconducting quantum circuits at the surface code threshold for fault tolerance *Nature* **508** 500–3
- [4] Kelly J *et al* 2015 State preservation by repetitive error detection in a superconducting quantum circuit *Nature* **519** 66–9
- [5] Wang Y, Li Y, Yin Z-Q and Zeng B 2018 16-qubit IBM universal quantum computer can be fully entangled *npj Quantum Inf.* **4** 46
- [6] Barends R *et al* 2016 Digitized adiabatic quantum computing with a superconducting circuit *Nature* **534** 222–6
- [7] Arute F *et al* 2019 Quantum supremacy using a programmable superconducting processor *Nature* **574** 505–10
- [8] Nielsen M A and Chuang I L 2000 *Quantum Computation and Quantum Information* (Cambridge: Cambridge University Press)
- [9] Rieffel E G and Polak W 2011 *Quantum Computing: A Gentle Introduction* (Cambridge, MA: MIT Press)
- [10] Grover L K 1996 A fast quantum mechanical algorithm for database search *Proc. of the 28th Annual ACM Symp. on Theory of Computing—STOC'96* (New York: ACM) pp 212–9
- [11] Aspuru-Guzik A, Dutoi A D, Love P J and Head-Gordon M 2005 Chemistry: simulated quantum computation of molecular energies *Science* **309** 1704–7
- [12] Babbush R, Wiebe N, McClean J, McClain J, Neven H and Chan G K L 2018 Low-depth quantum simulation of materials *Phys. Rev. X* **8** 011044
- [13] Jiang Z, Sung K J, Kechedzhi K, Smelyanskiy V N and Boixo S 2018 Quantum algorithms to simulate many-body physics of correlated fermions *Phys. Rev. Appl.* **9** 44036
- [14] Babbush R, Gidney C, Berry D W, Wiebe N, McClean J, Paler A, Fowler A and Neven H 2018 Encoding electronic spectra in quantum circuits with linear T complexity *Phys. Rev. X* **8** 41015
- [15] Shor P 1994 Algorithms for quantum computation: discrete logarithms and factoring *Proc. 35th Annual Symp. on Foundations of Computer Science* (Piscataway, NJ: IEEE) pp 124–34
- [16] Smelyanskiy V N, Kechedzhi K, Boixo S, Isakov S V, Neven H and Altshuler B 2018 Non-ergodic delocalized states for efficient population transfer within a narrow band of the energy landscape (arXiv:1802.09542)
- [17] Fowler A G, Mariantoni M, Martinis J M and Cleland A N 2012 Surface codes: towards practical large-scale quantum computation *Phys. Rev. A* **86** 032324
- [18] Boixo S, Isakov S V, Smelyanskiy V N, Babbush R, Ding N, Jiang Z, Bremner M J, Martinis J M and Neven H 2018 Characterizing quantum supremacy in near-term devices *Nat. Phys.* **14** 1–6
- [19] Bremner M J, Montanaro A and Shepherd D J 2016 Achieving quantum supremacy with sparse and noisy commuting quantum computations *Quantum* **1** 8
- [20] Neill C *et al* 2018 A blueprint for demonstrating quantum supremacy with superconducting qubits *Science* **360** 195–9
- [21] De Raedt K, Michielsen K, De Raedt H, Trieu B, Arnold G, Richter M, Lippert T, Watanabe H and Ito N 2007 Massively parallel quantum computer simulator *Comput. Phys. Commun.* **176** 121–36
- [22] Preskill J 2018 Quantum computing in the nisy era and beyond *Quantum* **2** 79
- [23] Smelyanskiy M, Sawaya N P D and Aspuru-Guzik A 2016 qHiPSTER: the quantum high performance software testing environment (arXiv:1601.07195)

- [24] Häner T and Steiger D S 2017 0.5 petabyte simulation of a 45-qubit quantum circuit *Proc. of the Int. Conf. for High Performance Computing, Networking, Storage and Analysis* (New York: ACM) pp 33
- [25] Aaronson S and Chen L 2016 Complexity-theoretic foundations of quantum supremacy experiments (arXiv:1612.05903)
- [26] Bouland A, Fefferman B, Nirkhe C and Vazirani U 2018 Quantum supremacy and the complexity of random circuit sampling (arXiv:1803.04402)
- [27] Pednault E, Gunnels J A, Nannicini G, Horesh L, Magerlein T, Solomonik E and Wisnieff R 2017 Breaking the 49-qubit barrier in the simulation of quantum circuits (arXiv:1710.05867)
- [28] Chen Z Y, Zhou Q, Xue C, Yang X, Guo G C and Guo G P 2018 64-qubit quantum circuit simulation *Sci. Bull.* **63** 964–71
- [29] Li R, Wu B, Ying M, Sun X and Yang G 2018 Quantum supremacy circuit simulation on Sunway TaihuLight (arXiv:1804.04797 [quant-ph])
- [30] Chen J, Zhang F, Huang C, Newman M and Shi Y 2018 Classical simulation of intermediate-size quantum circuits (arXiv:1805.01450 [quant-ph])
- [31] Markov I L, Fatima A, Isakov S V and Boixo S 2018 Quantum supremacy is both closer and farther than it appears (arXiv:1807.10749 [quant-ph])
- [32] Villalonga B, Boixo S, Nelson B, Henze C, Rieffel E, Biswas R and Mandrà S 2019 A flexible high-performance simulator for verifying and benchmarking quantum circuits implemented on real hardware *npj Quantum Inf.* **5** 1–16
- [33] De Raedt H, Jin F, Willsch D, Nocon M, Yoshioka N, Ito N, Yuan S and Michielsen K 2018 Massively parallel quantum computer simulator, eleven years later (arXiv:1805.04708)
- [34] McClure D and Gambetta J 2019 Quantum computation center opens (<https://www.ibm.com/blogs/research/2019/09/quantum-computation-center/>)
- [35] Aaronson S and Arkhipov A 2010 The computational complexity of linear optics *Proc. of the 43rd Annual ACM Symp. on Theory of Computing* (New York, NY: ACM) pp 333–42
- [36] Bremner M J, Montanaro A and Shepherd D J 2016 Average-case complexity versus approximate simulation of commuting quantum computations *Phys. Rev. Lett.* **117** 80501
- [37] Aaronson S and Chen L 2016 Complexity-theoretic foundations of quantum supremacy experiments *LIPICs-Leibniz Int. Proc. in Informatics vol 79* (Wadern: Schloss Dagstuhl Leibniz-Zentrum für Informatik)
- [38] Harrow A and Mehraban S 2018 Approximate unitary t-designs by short random quantum circuits using nearest-neighbor and long-range gates (arXiv:1809.06957)
- [39] Movassagh R 2018 Efficient unitary paths and quantum computational supremacy: a proof of average-case hardness of random circuit sampling (arXiv:1810.04681)
- [40] Bishop L S, Bravyi S, Cross A, Gambetta J M and Smolin J *Quantum Volume* Technical report, IBM T J Watson, 2017
- [41] Magesan E, Gambetta J M and Emerson J 2011 Scalable and robust randomized benchmarking of quantum processes *Phys. Rev. Lett.* **106** 180504
- [42] Knill E, Leibfried D, Reichle R, Britton J, Blakestad R, Jost J, Langer C, Ozeri R, Seidelin S and Wineland D 2008 Randomized benchmarking of quantum gates *Phys. Rev. A* **77** 012307
- [43] Magesan E, Gambetta J M and Emerson J 2012 Characterizing quantum gates via randomized benchmarking *Phys. Rev. A* **85**
- [44] Erhard A *et al* 2019 Characterizing large-scale quantum computers via cycle benchmarking (arXiv:1902.08543)
- [45] Britt K A, Mohiyaddin F A and Humble T S 2017 Quantum accelerators for high-performance computing systems 2017 *IEEE Int. Conf. on Rebooting Computing (ICRC)* pp 1–7
- [46] Humble T S, Sadler R J and Britt K A 2018 Simulated execution of hybrid quantum computing systems *Quantum Information Science, Sensing, and Computation X vol 10660* (Vienna International Society for Optics and Photonics) 1066002
- [47] Gottesman D 1998 The Heisenberg representation of quantum computers (arXiv:quant-ph/9807006)
- [48] Aaronson S and Gottesman D 2004 Improved simulation of stabilizer circuits *Phys. Rev. A* **70** 052328
- [49] Bravyi S and Gosset D 2016 Improved classical simulation of quantum circuits dominated by clifford gates *Phys. Rev. Lett.* **116** 250501
- [50] Bennink R S, Ferragut E M, Humble T S, Laska J A, Nutaro J J, Pleszkoch M G and Pooser R C 2017 Unbiased simulation of near-clifford quantum circuits *Phys. Rev. A* **95** 062337
- [51] Markov I L and Shi Y 2008 Simulating quantum computation by contracting tensor networks *SIAM J. Comput.* **38** 963–81
- [52] Biamonte J and Bergholm V 2017 Tensor networks in a nutshell (arXiv:1708.00006)
- [53] McCaskey A, Dumitrescu E, Chen M, Lyakh D and Humble T 2018 Validating quantum-classical programming models with tensor network simulations *PLOS ONE* **13** 1–19
- [54] Boixo S, Isakov S V, Smelyanskiy V N and Neven H 2017 Simulation of low-depth quantum circuits as complex undirected graphical models (arXiv:1712.05384 [quant-ph])
- [55] Boixo S and Neill C 2018 The question of quantum supremacy *Google AI Blog* <https://github.com/sboixo/GRCS>
- [56] Chen M-C, Li R, Gan L, Zhu X, Yang G, Lu C-Y and Pan J-W 2019 Quantum teleportation-inspired algorithm for sampling large random quantum circuits (arXiv:1901.05003 [quant-ph])
- [57] Lyakh D 2016 Tensor algebra library routines for shared memory systems (tal-sh) [https://github.com/DmitryLyakh/TAL\\_SH](https://github.com/DmitryLyakh/TAL_SH)
- [58] Lyakh D I 2015 An efficient tensor transpose algorithm for multicore cpu, intel xeon phi, and nvidia tesla gpu *Comput. Phys. Commun.* **189** 84–91
- [59] Hynninen A and Lyakh D I 2017 Cutt: a high-performance tensor transpose library for CUDA compatible gpus (arXiv:1705.01598)
- [60] Lyakh D I 2019 Domain-specific virtual processors as a portable programming and execution model for parallel computational workloads on modern heterogeneous high-performance computing architectures *Int. J. Quantum Chem.* **116** e25926
- [61] Zhang F *et al* 2019 Alibaba cloud quantum development kit: large-scale classical simulation of quantum circuits (arXiv:1907.11217)